Electronic Supplementary Information

Unprecedented Encapsulation of a $[Fe^{III}Cl_4]^-$ Anion in a Cationic $[Fe^{II}_4L_6]^{8+}$ Tetrahedral Cage Derived from 5,5′′′-Dimethyl-2,2′:5′,5′′:2′′,2′′′-quaterpyridine

Christopher R. K. Glasson,[a] Jack K. Clegg,[b,c] John C. McMurtrie,[d] George V. Meehan,*[a] Leonard F. Lindoy,*[a,b] Cherie A. Motti,[e] Boujemaa Moubaraki,[f] Keith S. Murray[f] and John D. Cashion[g]

[a] School of Pharmacy and Molecular Sciences, James Cook University, Townsville, Qld 4814, Australia. E-mail: George.Meehan@jcu.edu.au

[b] School of Chemistry, F11, The University of Sydney, NSW 2006, Australia. Fax: +61 2 93513329; E-mail: lindoy@chem.usyd.edu.au

[c] Department of Chemistry, The University of Cambridge, Lensfield Rd, Cambridge, UK, CB2 1EW.

[d] Chemistry, Queensland University of Technology, GPO Box 2434, Brisbane 4001, Qld. Australia.

[e] The Australian Institute of Marine Science, Townsville, 4810, Qld. Australia.

[f] School of Chemistry, Monash University, PO Box 23, Clayton, Vic, 3800 Australia.

[g] School of Physics, Monash University, PO Box 23, Clayton, Vic, 3800 Australia.

Section S1: X-ray analysis.

Data for **$[Fe_4(L)_6{\supset}FeCl_4](PF_6)_7{\cdot}12H_2O$** were collected with ω scans to approximately 56° 2θ using a Bruker SMART 1000 diffractometer employing graphite-monochromated Mo-K*a* radiation generated from a sealed tube (0.71073 Å). Data for **$[Fe_4(L)_6{\supset}FeCl_4](FeCl_4)_7{\cdot}3MeOH{\cdot}3MeCN{\cdot}9H_2O$** were collected on a Bruker-Nonius APEX2-X8-FR591 diffractometer employing graphite-monochromated Mo-Kα radiation generated from a rotating anode (0.71073 Å) with ω and ψ scans to approximately 65° 2θ.[1] All data were collected at 150(2) K. Data integration and reduction were undertaken with SAINT and XPREP.[2] Subsequent computations were carried out using the WinGX-32 graphical user interface.[3] Structures were solved by direct methods using SIR97.[4] Multi-scan empirical absorption corrections, when applied, were applied to the data set using the program SADABS.[5] Data were refined and extended with SHELXL-97.[6] In general, non-hydrogen atoms with occupancies greater than 0.5 were refined anisotropically. Carbon and alcohol-bound hydrogen atoms were included in idealised positions and refined using a riding model. Water hydrogen atoms could not be located in the difference Fourier map and were not modelled. Disorder was modelled using standard crystallographic methods including constraints and restraints where necessary.

$[Fe_4(L)_6 \supset FeCl_4](PF_6)_7 \cdot 12H_2O$: Formula $C_{132}H_{132}Cl_4F_{42}Fe_5N_{24}O_{12}P_7$, *M* 3682.46, cubic, space group $P\ \bar{4}_3n$(#218), *a* 21.7946(6), *b* 21.7946(6), *c* 21.7946(6) Å, *V* 10352.5(5) $Å^3$, D_c 1.181 g cm^{-3}, *Z* 2, crystal size 0.15 by 0.14 by 0.13 mm, colour red, habit tetrahedron, temperature 150(2) Kelvin, λ(MoKα) 0.71073 Å, μ(MoKα) 0.534 mm^{-1}, $T(SADABS)_{min,max}$ 0.825404, 1.0000, $2\theta_{max}$ 56.62, *hkl* range -28 28, -28 29, -28 27, *N* 95183, N_{ind} 4262(R_{merge} 0.0980), N_{obs} 2740(I > 2σ(I)), N_{var} 171, residuals* *R*1(*F*) 0.0596, *wR*2(F^2) 0.1827, GoF(all) 0.968, $\Delta\rho_{min,max}$ -0.792, 0.756 e^- $Å^{-3}$. Flack parameter[7] 0.01(4).

*$R1 = \Sigma||F_o| - |F_c||/\Sigma|F_o|$ for $F_o > 2\sigma(F_o)$; $wR2 = (\Sigma w(F_o^2 - F_c^2)^2/\Sigma(wF_c^2)^2)^{1/2}$ all reflections
$w=1/[\sigma^2(F_o^2)+(0.1243P)^2+0.0000P]$ where $P=(F_o^2+2F_c^2)/3$

$[Fe_4(L)_6 \supset FeCl_4](FeCl_4)_7 \cdot 3MeOH \cdot 3MeCN \cdot 9H_2O$: Formula $C_{47}H_{49}Cl_{10.667}Fe_4N_9O_4$, *M* 1405.49, cubic, space group $F2_3$(#196), *a* 29.6690(3), *b* 29.6690(3), *c* 29.6690(3) Å, *V* 26116.1(5) $Å^3$, D_c 1.072 g cm^{-3}, *Z* 12, crystal size 0.250 by 0.230 by 0.190 mm, colour red, habit prism, temp. 150(2) Kelvin, λ(MoKα) 0.71073 Å, μ(MoKα) 1.014 mm^{-1}, $T(SADABS)_{min,max}$ 0.6636, 0.7465, $2\theta_{max}$ 66.14, *hkl* range -43 45, -45 45, -44 45, *N* 107440, N_{ind} 8252(R_{merge} 0.0297), N_{obs} 7472(I > 2σ(I)), N_{var} 250, residuals* *R*1(*F*) 0.0482, *wR*2(F^2) 0.1456, GoF(all) 1.187, $\Delta\rho_{min,max}$ -0.433, 0.961 e^- $Å^{-3}$. Flack parameter[7] 0.492(15).

*$R1 = \Sigma||F_o| - |F_c||/\Sigma|F_o|$ for $F_o > 2\sigma(F_o)$; $wR2 = (\Sigma w(F_o^2 - F_c^2)^2/\Sigma(wF_c^2)^2)^{1/2}$ all reflections
$w=1/[\sigma^2(F_o^2)+(0.0921P)^2+21.0217P]$ where $P=(F_o^2+2F_c^2)/3$

Section S2: Selected HR-ESI-MS isotopic distributions.

The electrospray (ES) high resolution spectra were determined using a Bruker BioAPEX 47e mass spectrometer equipped with an Analytica of Branford model 103426 (Branford, CT) electrospray ionisation (ESI) source. Direct infusion of the samples (~0.2 mg/mL in MeOH) were carried out using a Cole Palmer 74900 syringe pump at a rate of 100 µL/h. N_2 (sourced from a Domnick Hunter UHPLCMS18 nitrogen generator, flow of 3 L/min and maintained at 200 °C) was used as the drying gas to assist in desolvation of the droplets produced by ESI from an on axis grounded needle directed to a metal capped nickel coated glass capillary approximately 1 cm away. Data reduction was performed using Bruker Daltonics XMASS ver. 7.0.3.0 software. All measurements were conducted in positive ion mode.

The mass spectrum of $[Fe_4\mathbf{L}_6 \supset Fe^{III}Cl_4](PF_6)_7$ is illustrated in Figure S2 a). A series of clusters of ions consistent with the loss of PF_6^- from the parent species $[Fe_4\mathbf{L}_6 \supset Fe^{III}Cl_4](PF_6)_7$, $[Fe_4\mathbf{L}_6](PF_6)_8$ and

$[Fe_4\mathbf{L}_6{\supset}Fe^{II}Cl_4](PF_6)_6$ were observed. Figure S2 b) portrays the theoretical and experimentally observed isotopic distributions of the +3 ions of the above parent species.

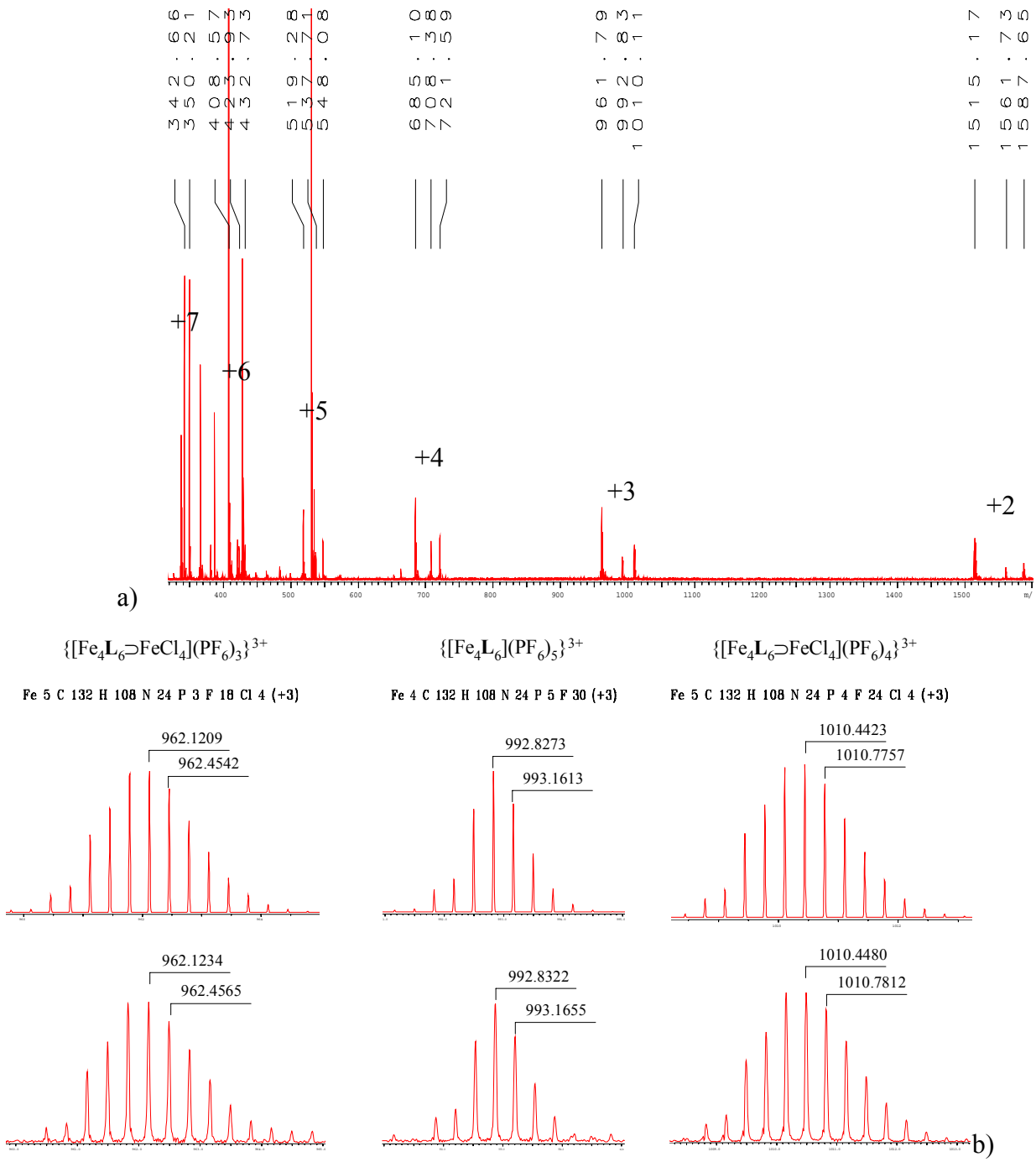

Fig. S2 a) The mass spectrum of $[Fe_4\mathbf{L}_6{\supset}Fe^{III}Cl_4](PF_6)_7$ (n = 6 or 7) showing the +2 to +7 ion clusters, and b) the calculated (top) and observed (bottom) isotopic distributions for the three +3 ions observed (formula shown above each).

Section S3: Cyclic Voltammetry and Oxidative Bulk Electrolysis of $[Fe^{II}{}_4L_6{\supset}Fe^{III}Cl_4](PF_6)_7.CH_3OH$

Initially the previously characterised species, $[Fe_4\mathbf{L}_6{\supset}BF_4](BF_4)_7.4H_2O$,[8] was used as a model to assess the intended experimental conditions for the exhaustive oxidation of $[Fe_4\mathbf{L}_6{\supset}FeCl_4](PF_6)_7.CH_3OH$. The CV of $[Fe_4\mathbf{L}_6{\supset}BF_4](BF_4)_7.4H_2O$ was determined employing an ~1 mM CH_3CN solution with 0.1 M tetrabutylammonium hexafluorophosphate as supporting electrolyte and a glassy carbon working electrode together with a silver wire reference electrode. The scan rate was varied from 50 to 100 mV s^{-1} with no significant change in the observed voltammograms. The CV showed a single wave ($E_{1/2}$= 1.14 V; ΔE_p= 99 mV; 4 e^-) under the above conditions employed (Fig. S3.1). An oxidative potential of 1.40 V was selected for the bulk electrolysis experiment.

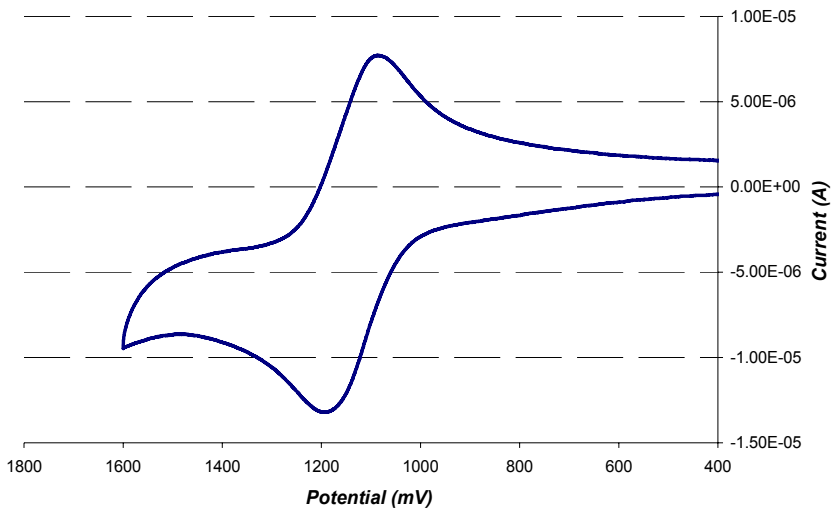

Fig. S3.1 The CV of $[Fe_4\mathbf{L}_6{\supset}BF_4](BF_4)_7.4H_2O$ with a scan rate of 100 mV s^{-1}.

The oxidative bulk electrolysis of $[Fe_4\mathbf{L}_6{\supset}BF_4](BF_4)_7.4H_2O$ (12.603 mg, 4.172 μmole) was conducted using a Pt mesh working electrode, Ag wire reference electrode and a Pt wire counter electrode, in 0.1 M tetrabutylammonium hexafluorophosphate (TBAF). The electrodes were separated by glass frits in an electrochemical cell. The oxidative potential was set to +1.40 V with the oxidative bulk electrolysis being discontinued when the current reached one percent of the initial current (Fig. S3.2). The experimentally determined measure of Q for the 4 e^- oxidation of $[Fe_4\mathbf{L}_6{\supset}BF_4](BF_4)_7.4H_2O$ was 1.547 C versus that of the theoretically determined value of Q, which was 1.611 C. This equates to 96 percent of the expected result for the 4 e^- oxidation of $[Fe_4\mathbf{L}_6{\supset}BF_4](BF_4)_7.4H_2O$.

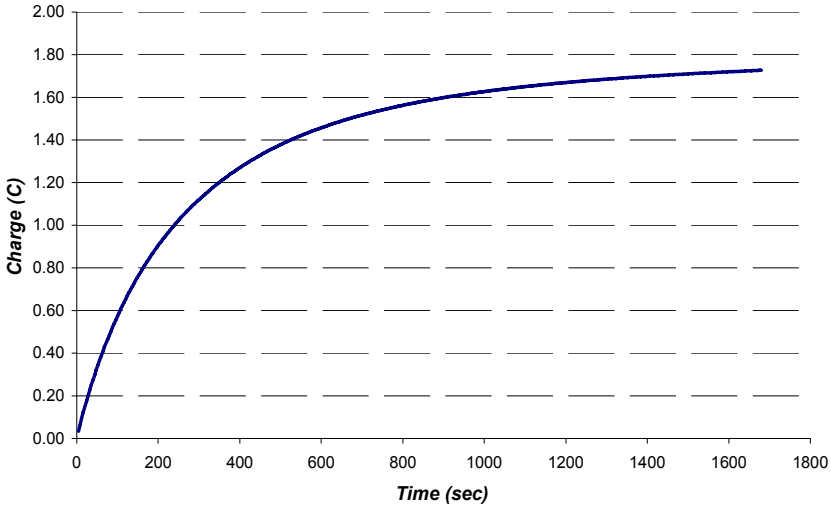

Fig. S3.2 The bulk electrolysis of $[Fe_4\mathbf{L}_6\supset BF_4](BF_4)_7$ using a oxidative potential of 1.40 V.

The CV of $[Fe_4\mathbf{L}_6\supset FeCl_4](PF_6)_7.CH_3OH$ was determined under the same conditions as those used for the collection of the $[Fe_4\mathbf{L}_6\supset BF_4](BF_4)_7.4H_2O$ CV. The CV showed a single wave with $E_{1/2}$ = 1.08 V and ΔE_p=111 mV; 4 e^- (Fig. S3.3). Based on this, an oxidative potential of 1.40 V was chosen for the bulk electrolysis experiment.

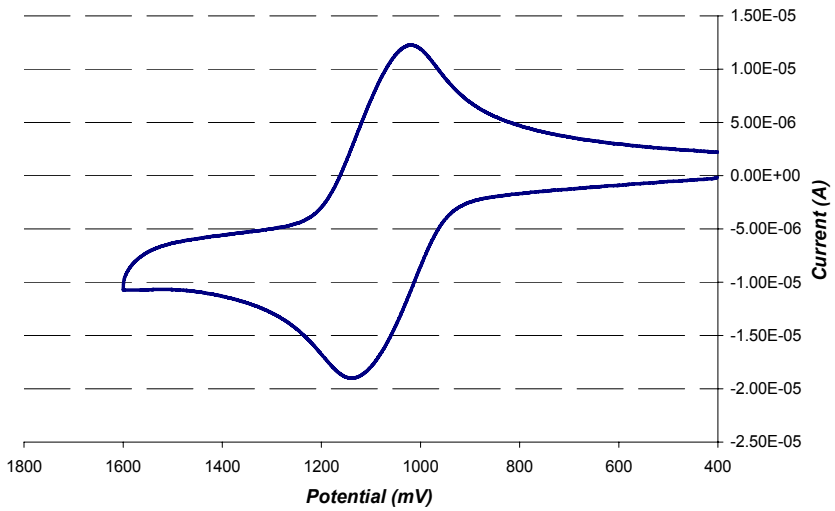

Fig. S3.3 The CV of $[Fe_4\mathbf{L}_6\supset FeCl_4](PF_6)_7.CH_3OH$ with a scan rate of 100 mV s^{-1}.

The oxidative bulk electrolysis of $[Fe_4\mathbf{L}_6\supset FeCl_4](PF_6)_7.CH_3OH$ (15.147 mg, 4.33 μmole) was performed as described for $[Fe_4\mathbf{L}_6\supset BF_4](BF_4)_7.4H_2O$ (Fig. S3.4). The initial deep red solution changed to light green at the completion of the experiment. The experimentally determined value of Q for the $4e^-$ oxidation of $[Fe_4\mathbf{L}_6\supset FeCl_4](PF_6)_7.CH_3OH$ was 1.692 C versus that of the theoretical value of 1.673 C. The former equates to 101 percent of the latter value.

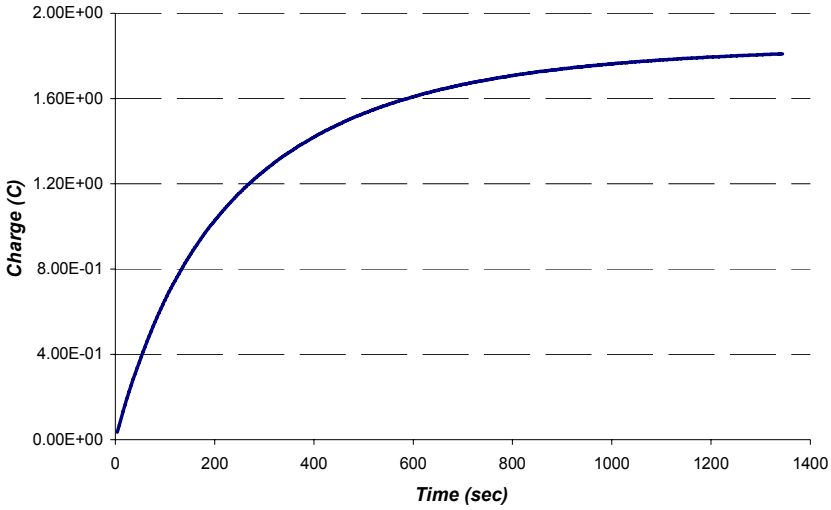

Fig. S3.4 The bulk electrolysis of $[Fe_4\mathbf{L}_6{\supset}FeCl_4](PF_6)_7.CH_3OH$ using a oxidative potential of 1.4 V.

Section S4: Magnetic susceptibility and Mössbauer details.

Magnetic susceptibilities were obtained on ~20 mg samples using a Quantum Design MPMS5 Squid instrument with a dc field of 1 T. The samples were contained in a calibrated gel capsule that was held in the centre of a soda straw, the latter being fixed to the end of the sample rod. The instrument was calibrated against a standard Pd sample and checked by use of a chemical calibrant, $CuSO_4.5H_2O$. Mössbauer effect spectra were obtained using a conventional constant acceleration drive with a symmetrical sawtooth waveform at room temperature (approximately 295 K) and at liquid nitrogen (78 K) temperatures. Isomer shift values are referenced relative to α-iron at room temperature and the velocity scale is also calibrated against α-iron. Fitting of spectra used both Voigtian and Lorentzian lineshape functions from the Recoil analysis software (Intelligent Scientific Applications Inc.).

Section S4: Synthesis of the inclusion complexes

$[Fe_4L_6{\supset}FeCl_4](PF_6)_7.CH_3OH$: A stirred solution of **L** (338 mg, 1 mmol) and $FeCl_2.5H_2O$ (217 mg, 1 mmol) in dry CH_3CN (30 cm^3). This reaction mixture was then refluxed for 24 hours resulting in a purple suspension. The solvent was removed under vacuum and the solid taken up in H_2O (30 cm^3) and stirred until the solid was completely dissolved (~1 h). The product was then precipitated by the addition of excess KPF_6 and was isolated by filtration. The red solid was purified by chromatography using sephadex LH-20 solid phase and acetonitrile as eluent to yield 270 mg (47 %) of product . This was dissolved in CH_3CN and set aside to recrystallise while MeOH diffusion into the solution took place; yield 130 mg (22 %) of product, part of which was used for microanalysis. UV/Vis (CH_3CN, nm): $\lambda_{max}(\varepsilon$ / dm^3 mol^{-1} $cm^{-1})$ = 251 (60 441), 271 (56 902), 320 (248 843), 532 (18 786); ^1H NMR (300 MHz, CD_3CN): δ = 2.19 (s),

6.75 (br s), 7.19 (br d), 7.50 (br s), 7.95 (br d), 8.37 (br d), 8.47 (br d); positive ion ESI-HRMS: (first series) m/z (M = $C_{132}H_{108}N_{24}P_6F_{36}Fe_5Cl_4$ in CH_3CN / MeOH): calcd for $[M - 2PF_6]^{2+}$: 1515.1637, found 1515.2444; calcd for $[M - 3PF_6]^{3+}$: 961.7875, found 961.8172; calcd for $[M - 4PF_6]^{4+}$: 685.0995, found 685.1147; calcd for $[M - 5PF_6]^{5+}$: 519.0866, found 519.0936; calcd for $[M - 6PF_6]^{6+}$: 408.4114, found 408.4162; (second series) m/z (M = $C_{132}H_{108}N_{24}P_8F_{48}Fe_4$ in CH_3CN / MeOH): calcd for $[M - 2PF_6]^{2+}$: 1561.7233, found 1561.7375; calcd for $[M - 3PF_6]^{3+}$: 992.8273, found 992.8278; calcd for $[M - 4PF_6]^{4+}$: 708.3793, found 708.3912; calcd for $[M - 5PF_6]^{5+}$: 537.7105, found 537.7178; calcd for $[M - 6PF_6]^{6+}$: 423.9313, found 423.9360; calcd for $[M - 7PF_6]^{7+}$: 342.6604, found 342.6648; (3rd series) m/z (M = $C_{132}H_{108}N_{24}P_7F_{42}Fe_5Cl_4$ in CH_3CN / MeOH): calcd for $[M - 2PF_6]^{2+}$: 1587.6458, found 1587.6503; calcd for $[M - 3PF_6]^{3+}$: 1010.1089, found 1010.1158; calcd for $[M - 4PF_6]^{4+}$: 721.3405, found 721.3487; calcd for $[M - 5PF_6]^{5+}$: 548.0795, found 548.0863; calcd for $[M - 6PF_6]^{6+}$: 432.5721, found 432.5766; calcd for $[M - 2PF_6]^{7+}$: 350.0668, found 350.0716; elemental analysis (%) calcd for $C_{132}H_{108}N_{24}P_7F_{42}Fe_5Cl_4.CH_3OH$ (3495.2444 g mol^{-1}): C 45.66, H 3.23, N 9.62, P 6.20; found: C 45.42, H 3.46, N 9.64, P 6.31.

$[Fe_4L_6 \supset FeCl_4](FeCl_4)_7.2CH_3OH.CH_3CN$: A mixture of **L** (228 mg, 0.67 mmol) and $FeCl_2.5H_2O$ (100 mg, 0.46 mmol) in CH_3OH (20 cm^3) was degassed with N_2 for 0.5 h. The reaction mixture was then heated with microwave energy in a sealed pressurised microwave vessel with temperature and pressure sensors and a magnetic stirrer bar (Step 1 – temperature ramped to 130 °C over 2 min using 400 W; step 2 – temperature held at 130 °C for 20 min using 30 % of 400 W). The reaction mixture was allowed to cool to room temperature and was filtered through celite to remove insoluble material. Excess saturated ether solution containing $HFeCl_4$[28] was added and the precipitate that formed was isolated by filtration, washed well with ether and dried under vacuum to afford the product (385 mg, 87 %) as a deep red solid. Thin layer chromatography on silica gel, with a mobile phase of CH_3CN, KNO_3 (aq) and water (7:0.5:1) indicated the presence of one major product. Crystalline material was obtained by diffusion of ether into a CH_3CN solution of the above product. UV/Vis (CH_3CN, nm): $\lambda_{max}(\varepsilon$ / dm^3 mol^{-1} cm^{-1}) = 320 (401 780), 532 (26 866); elemental analysis (%) calcd for $C_{132}H_{108}N_{24}Fe_{12}Cl_4.2CH_3OH.CH_3CN$ (3940.1938 g mol^{-1}): C 41.59, H 3.06, N 8.92; found: C 41.68, H 3.03, N 8.83.

Section S5: Variable temperature magnetic studies

The plot of μ_{eff}, per mol, for $[Fe_4\mathbf{L}_6 \supset Fe^{III}Cl_4](PF_6)\cdot CH_3OH$ is shown in Fig. S5.1 and is indicative of Curie-like behaviour for a d^5 $[Fe^{III}Cl_4]^-$ ion surrounded by four low-spin (t_{2g}^6) Fe^{II} ions within the Fe_4L_6 cage. Thus, at 300 K, the observed μ_{eff} value is 6.02 μ_B ($\chi_M T$ = 4.53 cm^3 mol^{-1} K), the small increase from spin-only (5.97 μ_B) being due to small second-order Zeeman (temperature independent paramagnetic susceptibility, TIP, 0.00015 cm^3 mol^{-1}, per Fe(II)) contributions from the Fe^{II} ions (expect μ_{eff}, per Fe_5, of

6.04 μ_B). The very small, gradual decrease in μ_{eff} noted between 300 and ~12 K, with a value of 5.96 μ_B occurring at the latter temperature, is due to the small TIP susceptibility being superimposed on the Curie susceptibility ($\chi = 4.375/T$) of the $Fe^{III}Cl_4^-$ ion. A small, more rapid decrease below 12 K is probably due to weak zero-field splitting effects for Fe^{III}. As anticipated, the magnetic data clearly support the inclusion of $Fe^{III}Cl_4^-$ (rather than, for example, $Fe^{II}Cl_4^{2-}$) in the tetrahedral host.

The μ_{eff} vs. T data for $[Fe_4\mathbf{L}_6{\supset}FeCl_4](FeCl_4)_7{\cdot}2CH_3OH{\cdot}CH_3CN$, per Fe_{12}, are shown in Figure S5.1. The moments remain essentially constant, at 16.19 μ_B, ($\chi_M T = 32.76$ cm^3 mol^{-1} K) between 300 and ~50 K, before decreasing, reasonably rapidly, to reach 13.1 μ_B at 4.2 K. The expected value of μ_{eff}, per Fe_{12}, for four low-spin Fe^{II} (see TIP discussion above) plus eight high-spin Fe^{III}, is 16.78 μ_B ($\chi_M T = 35.18$ cm^3 mol^{-1} K, a bit higher than is observed. The data are, never the less, generally supportive of the spin states/oxidation states proposed for this 'one-guest and seven ionic $Fe^{III}Cl_4^-$' derivative, the discrepancy possibly being due to loss of some solvent from the sample. The Mössbauer spectral data (below) also support the formulation. The decrease in μ_{eff} noted below ~50 K is possibly indicative of very weak spin coupling involving $Fe^{III}Cl_4^-$ ions (which is reflected by the presence of contacts between disordered encapsulated anions throughout the crystal packing), as well as zero-field splitting from eight d^5 ($^6A_1$) centres.

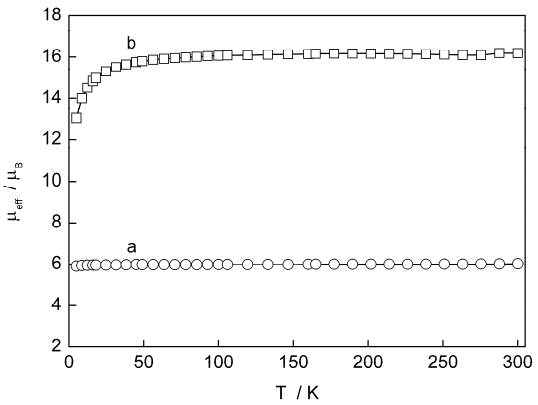

Fig. S5.1 The plots of magnetic moment μ_{eff}/μ_B, versus temperature (T / K) for a) $[Fe_4\mathbf{L}_6{\supset}FeCl_4](PF_6)_7{\cdot}CH_3OH$ and b) $[Fe_4\mathbf{L}_6{\supset}FeCl_4](FeCl_4)_7{\cdot}2CH_3OH{\cdot}CH_3CN$, (an applied dc field of 1 Tesla was used).

Mössbauer spectrosocopy was employed to corroborate the presence of the +III oxidation state of the iron in the included tetrachloroferrate species in both $[Fe_4\mathbf{L}_6{\supset}FeCl_4](PF_6)_7{\cdot}CH_3OH$ and $[Fe_4\mathbf{L}_6{\supset}FeCl_4](FeCl_4)_7{\cdot}2CH_3OH{\cdot}CH_3CN$. Both spectra, measured at 78 K, showed broad, asymmetric lineshapes, with no clear shoulders to unambiguously define the subspectra resulting from the ions forming the Fe(II) cage and the included/anionic $FeCl_4$ species. This is because the parameters for both Fe sites are, coincidentally, very similar. Thus extensive efforts were made to simulate the lineshapes by

means of Lorentzian or Voigtian functions and a number of possible alternative fits were obtained, with their associated best-fit minimisation parameter, and from which the preferred fit was deduced. What is clear is that the tetrahedral $FeCl_4$ anions are clearly Fe(III) in both compounds since the isomer shift, δ, and quadrupole splitting, ΔE_Q, parameters for $[Fe^{II}Cl_4]^{2-}$ are markedly different, viz. δ 0.92 mm s^{-1} and ΔE_Q 0.75 mm s^{-1} at 295 K.[9]

In the case of $[Fe_4\mathbf{L}_6{\supset}FeCl_4](PF_6)_7$, a very weak line at -1.2 mm s^{-1} (Figure S5.2) is clearly an impurity or of instrumental origin. Comparison of the δ and ΔE_Q values to those published for high-spin (HS) $FeCl_4^-$ (range δ 0.3 – 0.4 mm s^{-1} and ΔE_Q 0.3 – 0.4 mm s^{-1})[10] and for LS $Fe(bipy)_3^{2+}$ (δ 0.29 – 0.33 mm s^{-1}, ΔE_Q 0.3 – 0.4 mm s^{-1},[11] as well as the area ratios, helped to assign the constituent doublets (or singlets). The best-fit used two Lorentzian doublets, with a singlet for the weak impurity, and has the parameter set: doublet 1: δ = 0.38(1) mm s^{-1} and ΔE_Q = 0.66(1) mm s^{-1}, area % = 32, linewidth (FWHM) = 0.39(8) mm s^{-1}, assigned to $[Fe^{III}Cl_4]^-$; doublet 2: δ = 0.38(1) mm s^{-1} and ΔE_Q = 0.22(1) mm s^{-1}, area % = 64, linewidth = 0.40(9) mm s^{-1}, assigned to the equivalent four $Fe^{II}N_6$ sites forming the cage. The area ratio of 2 (Fe^{II} LS):1 (Fe^{III} HS) is less than that expected of 4:1.

For $[Fe_4\mathbf{L}_6{\supset}FeCl_4](FeCl_4)_7$, the 78 K spectrum is shown in Figure S5.2, and the best fit used three Lorentzian doublets and employed three similar isomer shifts, with one being due to impurity. The parameter set is : doublet 1: δ = 0.36(1) mm s^{-1} and ΔE_Q = 0.48(5) mm s^{-1}, area % = 61, linewidth (FWHM) = 0.54(8) mm s^{-1}, assigned to $[Fe^{III}Cl_4]^-$; doublet 2: δ = 0.34(1) mm s^{-1} and ΔE_Q = 0.18(4) mm s^{-1}, area % = 36, linewidth (FWHM) = 0.39(8) mm s^{-1}, assigned to $Fe^{II}N_6$ sites; doublet 3: δ = 0.30(5) mm s^{-1} and ΔE_Q = 1.1(1) mm s^{-1}, area % = 3, linewidth (FWHM) = 0.54(8) mm s^{-1}, assigned to impurity. The HS $[Fe^{III}Cl_4]^-$ doublet to LS $Fe^{II}N_6$ doublet area ratio of 2:1 is as anticipated. The parameter values for the included $[Fe^{III}Cl_4]^-$ and ionic $[Fe^{III}Cl_4]^-$ groups are the same in this fit. Despite these various nuances, the Mössbauer results support the magnetic and structural data on these two, closely related cage systems.

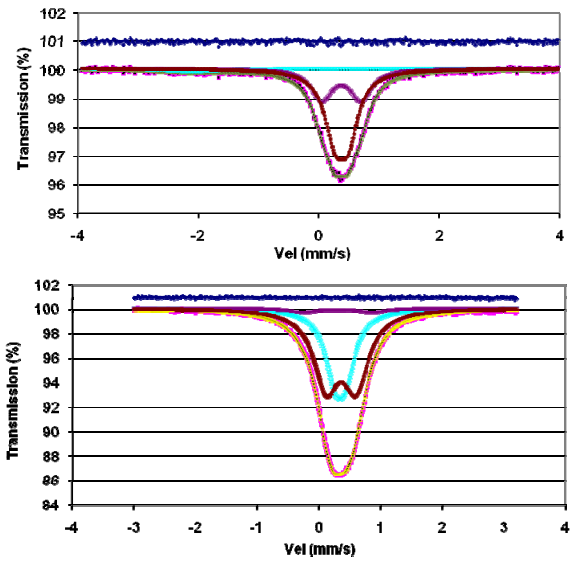

Fig. S5.2 The plots of Mössbauer effect spectra, at 78 K, for (top) $[Fe_4\mathbf{L}_6{\supset}FeCl_4](PF_6)_7.CH_3OH$ and (bottom) $[Fe_4\mathbf{L}_6{\supset}FeCl_4](FeCl_4)_7.2CH_3OH.CH_3CN$. The subspectra parameters are given in the text. The observed points are shown as ○. The top plots are the differences between calculated and observed points after best-fit in each case.

Section S6: References.

1 Bruker (1995), SMART, SAINT and XPREP. Bruker Analytical X-ray Instruments Inc., Madison, Wisconsin, USA ; Bruker-Nonius (2003). APEX v2.1, SAINT v.7 and XPREP v.6.14. Bruker AXS Inc. Madison, Wisconsin, USA.

2 Bruker (1995), SMART, SAINT and XPREP. Bruker Analytical X-ray Instruments Inc., Madison, Wisconsin, USA.

3 *WinGX-32: System of programs for solving, refining and analysing single crystal X-ray diffraction data for small molecules*, L. J. Farrugia, *J. Appl. Cryst.*, 1999, **32,** 837.

4 A. Altomare, M. C. Burla, M. Camalli, G. L. Cascarano, C. Giocavazzo, A. Guagliardi, A. G. C. Moliterni, G. Polidori and S. Spagna, *J. Appl. Cryst.,* 1999, **3**2, 115.

5 G. M. Sheldrick, *SADABS: Empirical Absorption and Correction Software,* University of Göttingen, Germany, 1999-2007.

6 G. M. Sheldrick, *SHELXL-97: Programs for Crystal Structure Analysis*, University of Göttingen, Germany, 1997.

7 H. D. Flack, *Acta Cryst*., 1983, **A39**, 876.

8 C. R. K. Glasson, G. V. Meehan, J. K. Clegg, L. F. Lindoy, P. Turner, M. B. Duriska and R.Willis, *Chem. Commun.*, 2008, 1190.

9 E. Styczeń, A. Pattek-Janczyk, M. Gazda, W. K. Jóźwiak, D. Wyrzykowski, and Z. Warnke, *Therm. Chim. Acta*, 2008, **480**, 30.

10 A. Proń, G. A. Fatseas, S. Krichène, S. LeFrant, F.Maurice and G. Froyer, *Phys. Rev. B*, 1985, **32**, 1839.

11 P. Kopel, Z. Trávniček, R. Zbořil and J. Marek, *Polyhedron*, 2004, **23**, 2193.